Global hydrometeor occurrence as observed by CloudSat: Initial observations from summer 2006

Gerald G. Mace,[1] Roger Marchand,[2] Qiquing Zhang,[1] and Graeme Stephens[3]

Received 6 December 2006; revised 4 February 2007; accepted 9 March 2007; published 8 May 2007.

[1] Measurements of global hydrometeor coverage and occurrence frequencies as observed by the cloud radar on CloudSat are summarized using data collected during Summer 2006. CloudSat was launched on 28 April 2006 and began collecting data routinely on 7 June 2006. In this article we document the distribution of cloudiness from the ITCZ to the Polar regions as observed by CloudSat during the first summer of operations. The overall global hydrometeor coverage as observed by CloudSat is found to be 0.506. The vertical distribution of zonally averaged hydrometeor occurrence shows the relationship of clouds with components of the atmospheric general circulation such as the Hadley Cell, the ubiquitous storms over the Southern Ocean, and the subtropical stratocumulus regimes.
Citation: Mace, G. G., R. Marchand, Q. Zhang, and G. Stephens (2007), Global hydrometeor occurrence as observed by CloudSat: Initial observations from summer 2006, *Geophys. Res. Lett.*, *34*, L09808, doi:10.1029/2006GL029017.

1. Introduction

[2] On April 28, 2006 NASA launched a pair of active remote sensors designed expressly for the mapping of hydrometeors and aerosols. CloudSat, carrying the Cloud Profiling Radar (CPR) [*Im et al.*, 2006], and CALIPSO (Cloud-Aerosol Lidar and Infrared Pathfinder Satellite Observation), fielding a two-channel lidar, were inserted into nearly identical orbits approximately 1 minute behind the NASA Earth Observing System (EOS) afternoon satellite known as Aqua. Together with the French satellite PARASOL and the EOS Chemistry satellite Aura which also fly very similar orbital tracks a few minutes behind CloudSat and CALIPSO, the A-Train satellite constellation has been formed [*Stephens et al.*, 2002] thus providing a unique ability to combine active and passive global observations of clouds.

[3] In this note we examine early results from the CloudSat Geometrical Profiling Product (hereafter referred to as Geoprof). Geoprof is one of the standard data products that will be produced by the CloudSat project. The Geoprof algorithm suite attempts to identify the location of hydrometeors in the earth's atmosphere using a cloud masking algorithm, estimate the atmospheric gaseous attenuation of the radar signal, and provides cloud identification information derived from Aqua MODIS data for use in data analysis and later cloud property retrieval algorithms. Detailed information about the Geoprof product can be found in the CloudSat Data Products Handbook (available at http://www.cloudsat.cira.colostate.edu/dataHome.php).

2. CPR and Cloudmask Description

[4] The CPR on CloudSat operates at a frequency of 94 GHz and points nominally in the nadir direction only. (Specific information about the CPR can also be found in the CloudSat Data Products Handbook.) The CPR emits a pulse of 3.3 microseconds in duration leading to a vertical resolution of approximately 480 m. The backscattered signal is oversampled to produce a range gate spacing of 240 m. From a 705 km orbit, the instantaneous field of view of the CPR at mean sea level is 1.4 km along and across track. 688 pulses are averaged to produce a nominal footprint of 2.5 km along track. We refer to the volume defined by this footprint and a 240 m range bin as a range resolution volume (RRV). The cloud masking algorithm is similar to the algorithm developed by *Clothiaux et al.* [1995, 2000] except that a power probability weighting scheme and an along-track integration scheme has been added. The CloudSat algorithm is described by R. T. Marchand et al. (Hydrometeor detection using CloudSat—An Earth orbiting 94 GHz cloud radar, submitted to *Journal of Atmospheric and Oceanic Technology*, 2006, hereinafter referred to as Marchand et al., submitted manuscript, 2006).

[5] Interpretation and analysis of CloudSat data require consideration of two issues. The mission requirement for the minimum detectable signal (MDS) is −28 dBZ at the beginning of the mission for nominal pulse averaging. Estimates since launch suggest an MDS between −30 dBZ and −32 dBZ. It was understood from the early stages of the mission design that the reflectivities of some clouds would be below the MDS. The intent is to determine the presence and properties of these low reflecting clouds using other A-Train observations. Some fraction of thin cirrus, mid-level liquid water clouds and non drizzling stratocumulus will not be observed by the CPR. Establishing the detection characteristics of the CPR, quantifying the fractions of the clouds missed, remains an ongoing research effort that will be reported in detail elsewhere.

[6] The other important issue is the nature of the data in the lowest approximately 1 km above the surface. Because the resolution volume is 480m, and the surface is typically two to five orders of magnitude more reflective than hydrometeors, measurements in the lowest two RRVs of a profile are dominated by backscattering from the surface. Surface contamination also extends above these lower two RRVs to approximately 1 km. Typically, it is only for the 5th RRV above the surface that the signal returns to the maximum

[1]Department of Meteorology, University of Utah, Salt Lake City, Utah, USA.
[2]Pacific Northwest National Laboratory, Richland, Washington, USA.
[3]Department of Atmospheric Sciences, Colorado State University, Fort Collins, Colorado, USA.

0094-8276/07/2006GL029017

sensitivity of the CPR. Only those hydrometeors that reflect above −10 dBZ in the 3rd and 4th RRVs (i.e. between about 480 and 960 m above the surface) will be detected above the surface contamination (on average). Deconvolving the surface influence from the 3rd and 4th RRVs above the surface is currently being investigated.

3. Hydrometeor Distributions During JJA 2006

[7] In Figure 1, we summarize the overall hydrometeor coverage through the depth of the troposphere as well as the layer base and top coverage in 3 height ranges during June–August 2006. Coverage in a vertical interval is defined as the number of profiles that contain an occurrence within the specified vertical interval divided by the total number of profiles collected in a given horizontal domain. In this analysis, hydrometeors are indicated by an RRV with a cloud mask value that ensures that the probability of false detection is reduced to less than 15% (Marchand et al., submitted manuscript, 2006). For Figures 1a and 2 the occurrence of hydrometeors anywhere in the column qualify that profile as containing hydrometeors while for the layer base and top maps (Figures 1b–1g), the occurrence of a distinct layer base (top) within that vertical interval qualify it as an occurrence. A cloud base (top) is defined when an RRV with cloudmask value indicating the presence of hydrometeors has an RRV with cloudmask indicating that hydrometeors are unlikely below (above) it.

[8] Figure 1 illustrates the unique view that CloudSat provides of the vertical distribution of hydrometeor occurrence in the global atmosphere. For instance, it has not been possible with conventional observations to depict the distribution of layer base-a quantity that is fundamental to constraining the radiative balance of the surface radiation budget [e.g., *Miller and Stephens*, 2001]. Together with layer top and overall hydrometeor coverage, a unique rendering of the hydrometeor distribution in the atmosphere is produced.

[9] Many established features of the global cloud distribution are readily identified in Figure 1. Figure 1a clearly shows the predominance of the inter tropical convergence zone (ITCZ) as a global feature that extends between 7° and 10°N. The distribution of layer bases throughout the ITCZ is nearly evenly distributed in the three vertical intervals depicted in Figure 1. However, layer tops in the ITCZ are predominantly above 10 km with a lesser frequency in the 5–10 km interval. Layer tops are rarely observed in the lower 3 km suggesting a predominance of cirrus, deep convection and cumulus congestus. The distribution of layer tops in the 5–10 km layer suggest that cumulus congestus is less likely in the Asian Monsoon region than in other regions of the ITCZ and are most likely to be found just north of Papua New Guinea and over tropical West Africa. The region near Burma ranks as the cloudiest location on Earth during the period considered.

[10] In the midlatitudes, the Southern Ocean is prominent with a nearly unbroken belt of cloudiness from 40°S–60°S with a notable extension into the South Pacific Convergence Zone (SPCZ) west of the dateline. Coverages in excess of 80% in many locations of the Southern Ocean are evident with intriguing layer structures throughout this region. Poleward of about 45°S, layers are predominantly based in the lower troposphere and extend into the 5–10 km layer-presumably frontal systems associated with Southern Ocean storms. Equatorward of this regime we find that while overall cloudiness decreases (except in the South Pacific) the layers become more prominently based in the middle and upper troposphere in a latitudinal band that displays a prominent break southeast of Australia near the longitude of New Zealand. East of this break the middle and upper troposphere-based layers are found more than 10° equatorward of their Indian Ocean location into the SPCZ where a high occurrence of cloud tops in excess of 10 km is also found. We speculate that this global structure is related to the equatorward extension of dissipating frontal zones associated with Southern Ocean storms. In the northern hemisphere midlatitudes some geographical structure is evident over continental locations while in the storm track regions of the North Atlantic and North Pacific, coverage exceeds 70% in many locations.

[11] Regarding specific cloud types and cloudiness regimes, our ability to identify layer base and top allows us to unambiguously distinguish, for instance, the global distribution of upper tropospheric clouds and oceanic stratocumulus with the caveats specific to CloudSat as discussed above. Figure 1f, for instance, shows the first unambiguous estimate of cloudiness based in the upper troposphere above 10 km (i.e., cirrus). Cirrus coverage is a maximum, as expected, over the western Pacific warm pool and extends into the Asian Monsoon region slightly north of the peaks in low based cloud occurrence. The oceanic stratocumulus regimes are also prominent features of Figure 1. The limitations of the CPR in the lowest 1 km are notable in the lack of cloudiness immediately west of the continents in subtropical latitudes. The occurrence of somewhat higher boundary layer cloudiness is clearly identified at other subtropical latitudes. This is especially true in the southern subtropics where we find prominent peaks in boundary layer cloud occurrence over the eastern ocean basins and the central Indian Ocean.

[12] Given the well known difficulties of identifying clouds with passive radiometry over snow and ice, active remote sensors provide observations of cloud coverage over the polar regions that are unaffected by the surface conditions or lack of solar reflection in the polar night (Figure 2). We find cloud cover exceeding 70% in much of the Artic north of the 75th parallel with an interesting minimum between the coastal regions of the Western Arctic extending from the western islands of the Canadian archipelago to the East Siberian Sea near 150°E. This minimum in CPR-observed cloud occurrence corresponds roughly to the region where sea ice retreats poleward during the summer season [*Francis and Hunter*, 2006]. As shown by *Key et al.* [2004], this area of seasonal open water has been found to contain heavy low-level stratus coverage that may not be detected by CloudSat. These observations suggest that cloud cover is small above this low level overcast and that the clouds become deeper poleward of the seasonal ice edge.

[13] Over Antarctica, the observed hydrometeor coverage generally decreases poleward of the coast. The elevated regions over the South Polar Plateau have lower observed cloud cover than the lower elevation regions of the western Antarctic. Other regions show very intriguing coverage statistics. For instance, we find that the Weddell Sea is

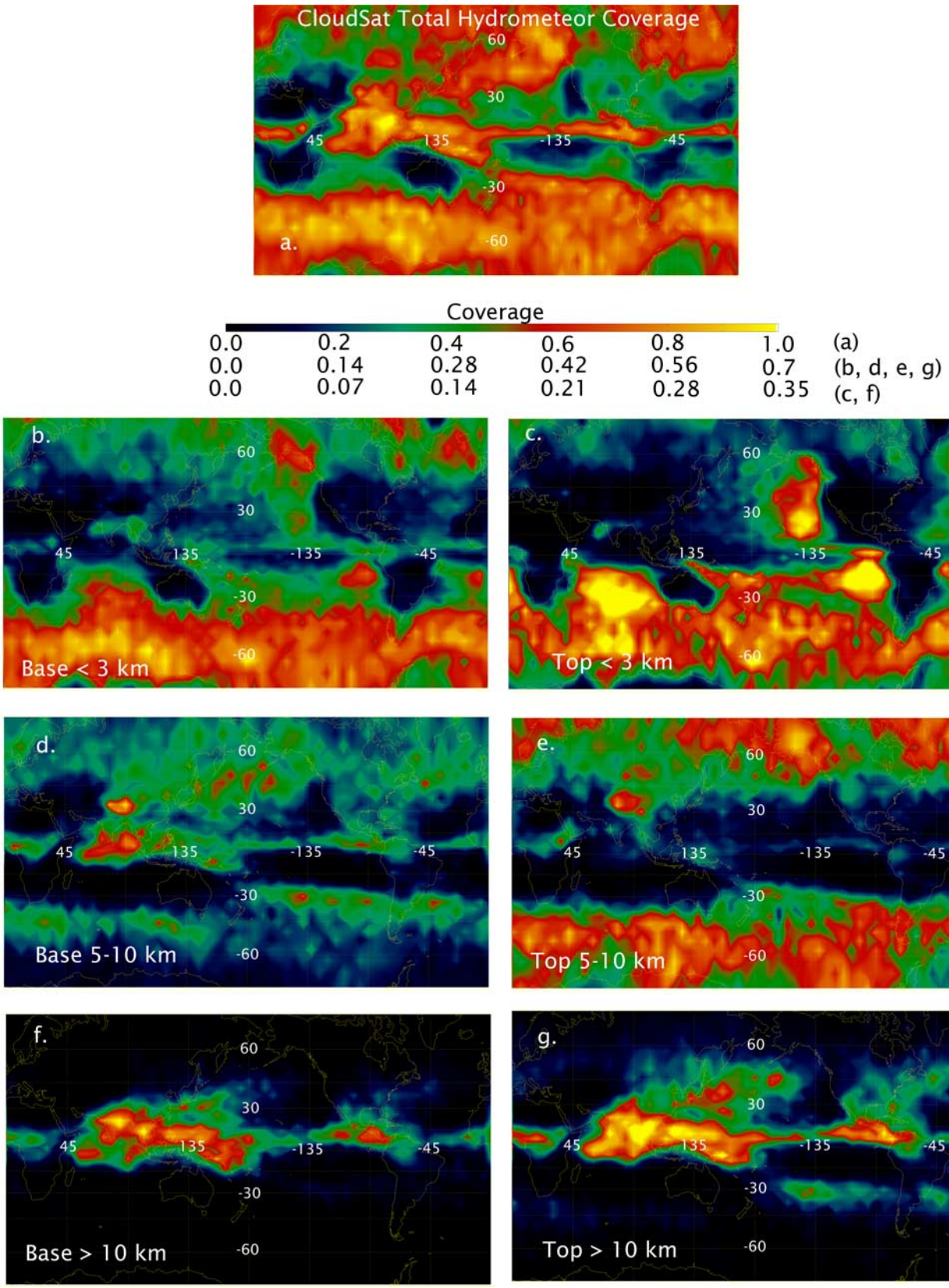

Figure 1. Hydrometeor coverage derived from CloudSat data collected during June, July, and August, 2006. 4° Latitude by 6° Longitude spatial averaging is used. Latitude and longitude lines are rendered every 15 degrees. (a) Total hydrometeor coverage. (b–g) Layer base and top coverage as specified in each figure.

significantly less cloudy than the Bellinghausen and Amundsen Seas west of the Antarctic Peninsula.

[14] Because the CPR on CloudSat is able to penetrate all but the most heavily precipitating hydrometeor layers, CloudSat is able to map the zonally averaged vertical distribution of hydrometeor occurrence (Figure 3). The most prominent features of this diagram are the branches of the Hadley Cell marked by the deep tropical cloud column centered near 7°N and the nearly cloud free region through the upper and middle troposphere centered along 12°S. Observed cloud occurrence in the ascending branch of the Hadley Cell in the lower and middle troposphere ranges between 30 and 40% while occurrence in the upper tropical troposphere is somewhat higher (~50%). Very high cloud occurrence exceeding 50% below 3 km is also noted through most latitudes of the southern hemisphere from the southern subtropical latitudes where high cloud occurrence is found below the otherwise very clear troposphere to where the occurrence peaks in association with storms over the Southern Ocean.

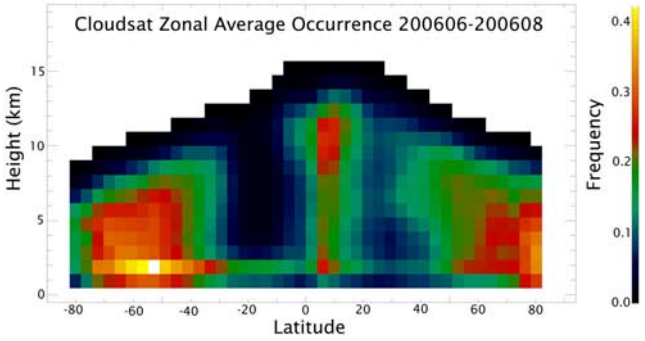

Figure 3. Zonally averaged occurrence frequency of hydrometeors as observed by CloudSat from data collected between June and August 2006. The vertical averaging interval is 1 km and the horizontal averaging interval is 2° Latitude.

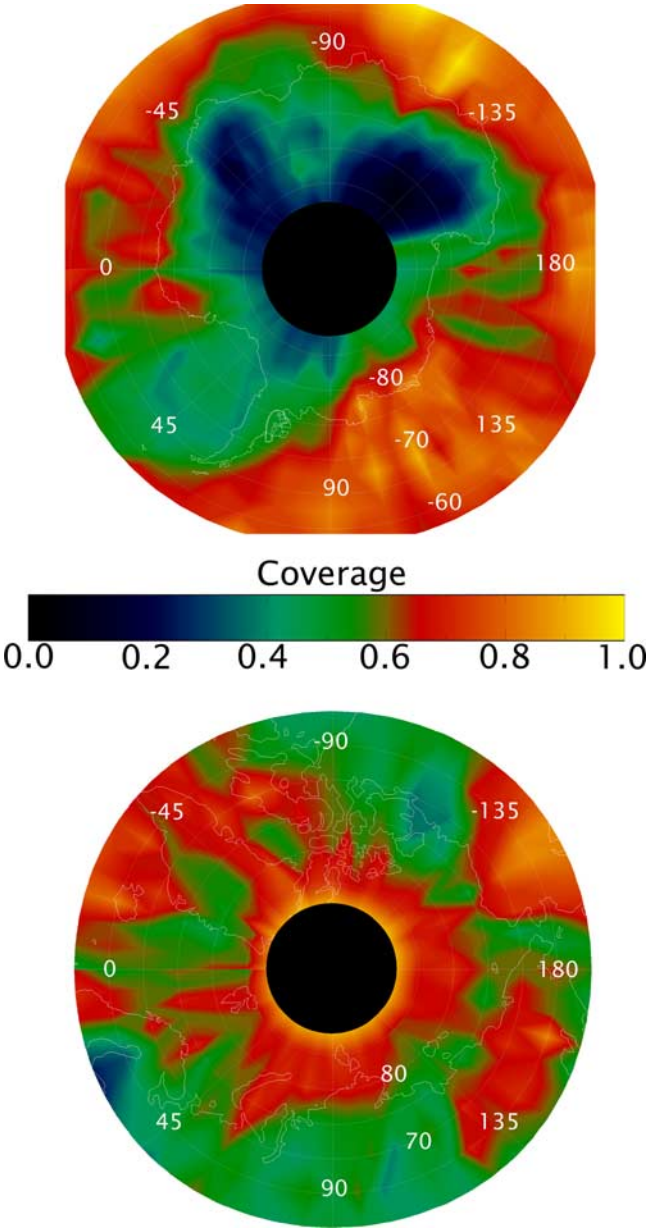

Figure 2. As in Figure 1a except that cloud occurrence over the north and south polar regions is shown.

4. Final Remarks

[15] This initial examination of CloudSat data from the first summer of operations provides an intriguing glimpse of the inner structure of the atmospheric hydrological cycle. Contained within the growing data set is information on the physical properties of clouds and precipitation as they relate directly to the individual weather systems in which they exist and more generally to elements of the atmospheric general circulation and the earth's energy balance.

[16] In this initial analysis, we have analyzed more than 40 million profiles from the beginning of the data collection period on 7 June through the end of August, 2006. We find that 0.506 of the profiles contain radar echo from hydrometeors suspended in the Earth's atmosphere with 0.17 of those profiles containing more than 1 hydrometeor layer. A very small fraction of the cloudy profiles are fully attenuated by precipitation (0.003) while 0.05 of the hydrometeor-containing profiles have layer thickness greater than 10 km, indicative of deep convection. These statistics need to be considered with respect to the specific observational constraints of the CPR as discussed in section 2.

[17] As a major component of the A-Train satellite constellation, CloudSat data will be combined with lidar measurements from CALIPSO to produce an authoritative mask of hydrometeor coverage, and then in combination with other passive measurements from Aqua, Aura, and PARASOL, the synergy of multi spectral active and passive sensing can be fully exploited.

[18] **Acknowledgments.** We would like to acknowledge the effort and dedication of the engineers and scientists at the Jet Propulsion Laboratory, Ball Aerospace, and the Cooperative Institute for Research in the Atmosphere (CIRA) for taking cloudsat from an idea to a reality. Support for this work was provided by NASA through a contract issued by the Jet Propulsion Laboratory, California Institute of Technology under a contract with NASA.

References

Clothiaux, E. E., M. A. Miller, B. A. Albrecht, T. P. Ackerman, J. Verlinde, D. M. Babb, R. M. Peters, and W. J. Syrett (1995), An evaluation of a 94-GHz radar for remote sensing of cloud properties, *J. Atmos. Oceanic. Technol.*, *12*, 201–229.

Clothiaux, E. E., T. P. Ackerman, G. G. Mace, K. Moran, R. T. Marchand, M. A. Miller, and B. E. Martner (2000), Objective determination of cloud heights and radar reflectivities using a combination of active remote sensors at the ARM CART sites, *J. Appl. Meteorol.*, *39*, 645–665.

Francis, J. A., and E. Hunter (2006), New insight into the disappearing Arctic sea ice, *Eos Trans. AGU*, *87*, 509.

Im, E., S. L. Durden, and C. Wu (2006), Cloud profiling radar for the CloudSat mission, *IEEE Aerosp. Electron. Syst. Mag.*, *20*, 15–18.

Key, E. L., P. J. Minnett, and R. A. Jones (2004), Cloud distributions over the Arctic Ocean: Surface-based and satellite observation, *Atmos. Res.*, *72*, 57–88.

Miller, S. D., and G. L. Stephens (2001), CloudSat instrument requirements as determined from ECMWF forecasts of global cloudiness, *J. Geophys. Res.*, *106*, 17,713–17,733.

Stephens, G. L., et al. (2002), The CloudSat mission and the A-train, *Bull. Am. Meteorol. Soc.*, *83*, 1771–1790.

G. G. Mace and Q. Zhang, Department of Meteorology, University of Utah, Salt Lake City, UT 84112, USA. (mace@met.utah.edu)

R. Marchand, Pacific Northwest National Laboratory, Richland, WA 99352, USA.

G. Stephens, Department of Atmospheric Sciences, Colorado State University, Fort Collins, CO 80523, USA.